Chinese Chemical Letters 35 (2024) 108485

Contents lists available at ScienceDirect

Chinese Chemical Letters

journal homepage: www.elsevier.com/locate/cclet

Defect-manipulated magnetoresistance and above-room-temperature ferromagnetism in two-dimensional $BaNi_2V_2O_8$

Pengfei Tan[a], Chuanhui Zhu[a,b,*], Jinjin Yang[a], Shuang Zhao[a], Tao Xia[a], Mei-Huan Zhao[a], Tao Han[a], Zheng Deng[c], Man-Rong Li[a,d,*]

[a] Key Laboratory of Bioinorganic and Synthetic Chemistry of Ministry of Education, School of Chemistry, Sun Yat-sen University, Guangzhou 510006, China
[b] School of Science and Engineering, The Chinese University of Hong Kong, Shenzhen 518172, China
[c] Institute of Physics, Chinese Academy of Sciences, Beijing 100190, China
[d] School of Science, Hainan University, Haikou 570228, China

ARTICLE INFO

Article history:
Received 5 February 2023
Revised 3 April 2023
Accepted 19 April 2023
Available online 21 April 2023

Keywords:
Layered honeycomb oxide
Topochemical reduction
Oxygen vacancies
Ferromagnetism
Magnetoresistance

ABSTRACT

The intricate correlation between multiple degrees of freedom and physical properties is a fascinating area in solid state chemistry and condensed matter physics. Here, we report a quantum-magnetic system $BaNi_2V_2O_8$ (BNVO), in which the spin correlation was modulated by unusual oxidation state, leading to different magnetic behavior. The BNVO was modified with topochemical reduction (TR) to yield TR-BNVO with partially reduced valance state of Ni^+ in the two-dimensional NiO_6-honeycomb lattice. Accordingly, the antiferromagnetic order is suppressed by the introduction of locally interposed Ni^+ and oxygen vacancies, resulting in a ferromagnetic ground state with the transition temperature up to 710 K. A positive magnetoresistance (7.5%) was observed in the TR-BNVO at 40 K under 7 T. These findings show that topological reduction is a powerful approach to engineer low-dimensional materials and accelerate the discovery of new quantum magnetism.

Transition metal (TM) oxides exhibit unique correlations between multiple degrees of freedom (lattice, charge, orbital and spin), which induce various exotic properties, such as colossal magnetoresistance, multiferroics, superconductivity, and others [1–5]. This feature can be ascribed to the strong interactions in TM oxides, where multiple interplays can be manipulated by altering the crystal structure and chemistry space. Therein, exotic valence state has been found to play a vital role for coupled behavior, by influencing the spin state and local electronic configuration, and thus governing the correlated interactions [6–8]. For example, the rare Ag^{2+} in two-dimensional (2D) $AgRuO_3$ is found to be responsible for its exotic magnetic behavior. In $AgRuO_3$, unprecedented charge transfer between Ag and Ru is ignited under high pressure, leading to a successive insulator-metal-insulator transition upon pressing [9]. Besides the pressure effect, low temperature topochemical reduction (TR) reaction can also enable the formation of metastable materials with unusual oxidation states and/or coordination geometries [10]. The nature and strength of the multiple coupling between metal centers strongly depend on the local electronic configuration and exchange interaction, which can be tuned by TR *via* anionic deintercalation, providing opportunities to explore complex TM oxides with exotic behavior. Along this line, metastable oxides with unusual local electronic configurations have been synthesized to explore exotic properties, such as square-planar Ir^{2+} [11], Ru^{2+} [12], Rh^+ [13], or Ni^+ [14]. $SrFeO_2$ adopted an infinite layered structure, which contains FeO_4 square-planar coordination, can be synthesized by TR from cubic $SrFeO_3$, displaying a magnetic transition temperature above 470 K [15]. More intriguingly, the search for nickelates with cuprate-like electronic structure (Ni^+), owing to the same d^9 electronic configuration and square-planar surroundings as in the Cu^{2+} analogs [16–18]. For example, the locally unusual Ni^+ in Sr-doped $NdNiO_2$ ($Nd_{0.8}Sr_{0.2}NiO_2$) film, the so-called 'infinite-layer' nickelate, demonstrates an exotic superconducting response [19]. The undoped $Nd_6Ni_5O_{12}$ film also exhibits superconductivity, in which the optimal cuprate-like $d^{8.8}$-stae is achieved without chemical doping [20]. These findings emphasize the key role of unusual electronic configuration for emergent exotic properties.

As one of the most intriguing 2D quantum system, $BaA_2B_2O_8$ (A = Co, Mn, Cu, Ni, Fe; B = P, As, V) has drawn considerable attention due to their unique magnetic models, such as one-dimensional (1D) Haldane chain and 2D Kitaev models [21–23]. These mag-

* Corresponding authors.
E-mail addresses: zhuchuanhui@cuhk.edu.cn (C. Zhu), limanrong@mail.sysu.edu.cn (M.-R. Li).

https://doi.org/10.1016/j.cclet.2023.108485
1001-8417/

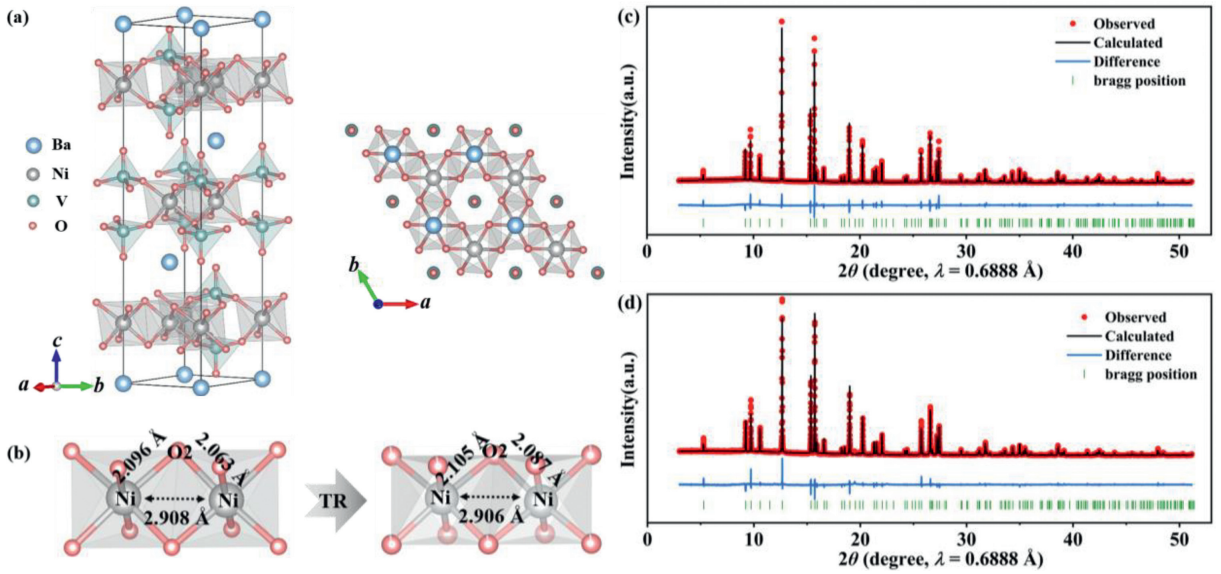

Fig. 1. (a) The crystal structure of BNVO phase. (b) Comparison of the local structure change of Ni-O coordination. (c, d) Refinements of the SPXD data of BNVO and TR-BNVO, the experimental, calculated, difference curves, and Bragg-reflection positions are shown in red, black, blue and green, respectively.

nets exhibit quantum critical phenomena ranging from conventional long-range or short-range magnetic order, spin "solids", to spin "liquids" [24–27]. The Co-based 2D-honeycomb layered $BaCo_2As_2O_8$ (space group (S. G.) of *R*-3) shows weak-field induced nonmagnetic state, implying the presence of strong magnetic frustration and weak non-Kitaev interactions [28]. The 1D-Ising-like antiferromagnetic (AFM) spin chain in $BaCo_2V_2O_8$ (S. G. of $I4_1/acd$) renders magnetic-field induced topological quantum phase transition, giving an experimental realization for the hotspot of topological excitations [29]. Further studies show that the spin correlations can be tuned by disordering the 2D honeycomb lattice in $BaCo_2(P_{1-x}V_x)_2O_8$, uncovering a promising candidate system for quantum spin-liquid [30]. Here, motivated by conspicuous theoretical models, we revisit one of the $BaA_2B_2O_8$ materials, $BaNi_2V_2O_8$ (BNVO), which is the 2D spin-1 honeycomb layered antiferromagnet [31]. BNVO can be considered as a nearly perfect realization of the 2D *XY* model, which undergoes topological phase transition (Berezinskii-Kosterlitz-Thouless transition, BKT) caused by the unbinding of vortex-antivortex pair excitations [32,33]. The introduction of vacancies into the anion sublattice often gives rise to alteration of physical properties, including ionic and electronic conductivity, magnetic order, and/or magnetoelectric behavior, which is modulated by exchange interactions *via* bridging anions. In light of the layered honeycomb lattice of BNVO with unusual ground state, the introduction of oxygen vacancies in the geometrically frustrated honeycomb lattices is expected to give rise to exotic physical behavior in a Ni^{+}-Ni^{2+} mixed Kitaev model. Here, we present comprehensive studies on the magnetic and magnetoelectric behaviors of BNVO with unusual oxidation states of Ni by TR reaction.

The mixed $Ni^{+/2+}$ spin states in the layered honeycomb lattice of TR-BNVO is experimentally realized by the reaction of BNVO with CaH_2 at 623 K. The phase and purity of the synthesized BNVO and TR-BNVO were firstly assessed by powder X-ray diffraction (PXD, SmartLab SE diffractometer, Rigaku, Japan) measurements (Fig. S1 in Supporting information). The diffraction peaks of TR-BNVO are matched well with those of the BNVO with a slightly shift to higher angle range, indicating the overall sublattice of TR-BNVO is retained in the 2D-honeycomb matrix (Fig. 1a). Controllable experiments were also performed to explore the boundary of reduction degree. Therein, excess CaH_2 is beneficial to promote the TR reaction of the oxide. The reaction process cannot be driven under lower temperature. Longer reaction time and higher temperature would result in precursor decomposition. In order to precisely distinguish the content of oxygen vacancy (V_O), thermogravimetric analysis (TGA) was further performed to the TR-BNVO in air (Fig. S2 in Supporting information). The mass increment began at around 500 K and ended at about 1100 K, displaying a weight increase percentage of $\Delta m/m$ ~1.16%, which underlies the formula of TR-BNVO being $BaNi_2V_2O_{7.65}$ and indicates ~4.4% V_O of the anionic sites. After TGA measurements, the powder color changed from black into yellow, which is consistent with the as-made BNVO.

Compared with conventional laboratory PXD, Synchrotron powder X-ray diffraction (SPXD) provides better sensitivity and resolution, thus improving the identification of crystalline structures. As shown in Figs. 1c and d, the collected SPXD data of BNVO and TR-BNVO were comparably refined to yield reasonable crystallographic information, therein the content of V_O was fixed by the TGA results [34]. Corresponding crystallographic information are listed in Tables S1-S3 (Supporting information). The crystal structure of BNVO is well consistent with that reported by Rogado *et al.* (Fig. 1a) [31], which is a 2D lattice consisting of honeycomb layers of edge-sharing octahedral NiO_6 (Ni^{2+}, d^8) sheets, separated by nonmagnetic isolated VO_4 (V^{5+}, d^0) tetrahedra and Ba ions. The Ni-O bond length is divided into two groups (Ni-O2 ~2.096 Å and Ni-O2 ~2.063 Å). The intralayer Ni-Ni distance is 2.908 Å (superexchange interaction between two adjacent Ni ions *via* bridged O). Thus, the magnetic ground state of BNVO is expected to be determined by the Ni^{2+}-O-Ni^{2+} coupled interactions for AFM order. After TR, V_O is introduced into the lattice with a slight contraction (0.03% by unit cell volume *V*) in unit cell (*R*-3, $a = 5.0307(1)$ Å, $c = 22.3514(2)$ Å, $V = 489.88(1)$ Å^3). To distinguish the location and content of V_O, we tested the deviation of the oxygen content for TR-BNVO by refining the occupancy factors *g* of different O site. The refinements for g_{O1} and g_{O2} were 0.993(7) and 0.939(1) respectively, indicating that the V_O tends to appear at the O2 site. Further refinements for g_{O2} solely did not diminish the refinement results. Therefore, we conclude that the V_O is introduced at O2 site, refined to be about 4.2%, which is in reasonable agreement with that (4.4%) from TGA analysis on TR-BNVO. In addition, the emerged V_O ignites increased electrons for the adjacent metal sites, leading to reduced valence state as evidenced by the elongated Ni-O bond length (Fig. 1b, Ni-O2 ~2.105 Å and Ni-O2 ~2.087 Å).

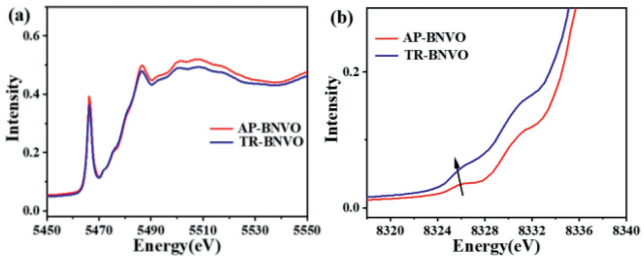

Fig. 2. Normalized (a) V *K*-edge and (b) Ni *K*-edgein the XANES of BNVO and TR-BNVO for comparison.

Generally, longer Ni-O bond length mean lower oxidation states of Ni considering the ionic radius at different valance state. The slightly increasing of Ni-O bond length can be observed in those reported for the $La_3Ni_2O_6$ ($n=2$) and $La_4Ni_3O_8$ ($n=3$) phases with the nominally average $Ni^{1.33+}$ oxidation state, signifying the mixed Ni^{+}/Ni^{2+} in the TR-BNVO [6,7,35]. As for the V site, the significant difference of ionic radius of the V can be observed in the same coordination environment, like 0.79, 0.64, 0.58, and 0.54 Å for V^{2+}, V^{3+}, V^{4+} and V^{5+}, respectively, indicating the changed oxidation state could be revealed by the correspond V-O bong length [36]. Hence, the almost unchanged bond length (~0.003 Å contraction of average bond length after TR) suggests that the oxidation state of V tends to maintain the initial +5, which is further confirmed by the bond valence sum (BVS) calculations. Thus, the ground state of TR-BNVO is still governed by the 2D $Ni^{+/2+}$-O-$Ni^{+/2+}$ exchange interaction. Mostly, the introduction of V_O into the anionic sublattice is prone to either decompose or revert back to the unreduced-counterpart when heated in air [37]. And the phase stability of TR-BNVO was further examined by the *in situ* VT-PXD measurements (Fig. S3 in Supporting information). After annealing in air, TR-BNVO would be gradually oxidized and completely converted back to the as-made state (Fig. S1). Clearly, the lattice parameter almost increases linearly in the whole temperature range with a transition point at around 900 K (Fig. S3b), which could be ascribed to the different thermal expansion coefficient between BNVO and TR-BNVO with the oxygen vacancies.

To gain deep insight into the valence states and local coordination of cations, we performed X-ray absorption near-edge spectroscopy (XANES) on TR-BNVO. Both the structure and the chemical shifts of the near edge structure are sensitive to the valence and local atomic environment. One signature of decreasing TM valence states (increasing *d*-count) is the chemical shift of the peak feature to lower energy as illustrated by the prominent shift between the metal and oxide spectra [38–40]. Fig. 2 displays the V- and Ni-*K* near edge of BNVO and TR-BNVO for comparison. As shown in Fig. 2a, the pre-edge features in BNVO and TR-BNVO spectra clearly overlap, indicating the unchanged V^{5+} in these oxides. This could also be manifested by the BVS calculations of V, where that of BNVO and TR-BNVO is 5.001(9) and 5.046(2), respectively. Noteworthy, with the introduction of V_O, the Ni-*K* near edge of TR-BNVO diverges slightly compared with that of BNVO, and skews toward the lower energies, thereby indicating the partial reduction of Ni valence from +2 toward +1 [41]. Thus, charge neutrality in TR-BNVO dictates mixed oxidation states of Ni^{+}/Ni^{2+}, providing the underlying opportunity for exotic behavior. To further investigate the local environment of BNVO and TR-BNVO, we collected the UV-vis absorption spectroscopy (Fig. S4 in Supporting information). Obviously, significant difference of the absorption band among BNVO and TR-BNVO can be observed at 500–700 nm with breaking point at 575 and 625 nm, respectively. This may be likely related to the modification of crystal structure and coordination environment. The optical band gap can be deduced from the absorption coefficient, α, where the intercept of the extrapolated linear plot of $(\alpha h\nu)^2$ and $(\alpha h\nu)^{1/2}$ versus photon energy ($h\nu$) yields the direct and indirect optical band gaps, respectively. As displayed in Fig. S4, the direct band gap of BNVO and TR-BNVO is estimated to be 2.24 and 0.81 eV, respectively. The prominent reduction of band gap in TR-BNVO could be ascribed to the introduction of oxygen vacancies, which might induce the formation of defect state. The narrower band gap of TR-BNVO than that of BNVO is also uncovered by the color evolution from yellow (BNVO) to black (TR-BNVO).

As a nearly perfect realization of the 2D *XY* model, BNVO has been comprehensively studied on the magnetic properties. Fig. 3a illustrates the temperature-dependent zero-field-cooled (ZFC) and field-cooled (FC) magnetization (*M-T*) curves of polycrystalline BNVO from 10 K to 300 K at 0.1 T. As expected, the temperature-dependent magnetization of BNVO is nearly identical to that reported in literatures [31]. Accompanied with decreasing temperature, the magnetization curve evolves with a broad peak centered at around 125 K, indicating a low-dimensional magnetic order. Further studies unveiled an AFM transition temperature at ~46 K [32]. After introducing V_O into the honeycomb lattice, mixed spin states (Ni^{+} in $S=1/2$ and Ni^{2+} in $S=1$) are created in the layers, leading to exchange disorder with modified inter- and intra-layer coupling. As displayed in Fig. 3b, the 2D AFM magnetic order at low temperature range is suppressed by the mixed spins, leading to a ferromagnetic (FM) ground state with transition temperature up to 710 K. The first derivative of ZFC curve is also plotted in Fig. S5 (Supporting information). Clearly, a ferromagnetic to paramagnetic transition could be seen around 710 K, which is identified by the minimum of dM/dT curve. This transition is ascribed to the exotic ferromagnetic order in the TR-BNVO. The dominating FM interactions are further evidenced by the isothermal $M(H)$ curves in Figs. 3c and d at different temperatures. Compared with the curves of BNVO, TR-BNVO exhibits obvious hysteresis loops in all measured temperatures, confirming the FM order is introduced in the mixed valence 2D honeycomb lattice. The emergent FM magnetic order far above room temperature is induced by modified exchange interactions between the adjacent Ni ion spins, *i.e.*, the double exchange (DE) and the super exchange (SE). For the as-made BNVO with Ni^{2+}-O-Ni^{2+} configuration, the SE interactions dominates in the 2D AFM order lattice. With the introduction of oxygen vacancies, the nominal Ni valence state is partially reduced to Ni^{+} ($S=1/2$), and thus mixed spin states is imported in the honeycomb lattice. At this state, TR-BNVO exhibits a Ni^{+}-O-Ni^{2+} configuration governed by DE interactions, therefore a FM order emerged as evidenced by the *M-T* curves. In addition, the slope of dM/dT curve presents a distinct change below 100 K (Fig. S5), which could be ascribed to the inhomogeneous phase induced by the random distribution of Ni^{+} and Ni^{2+} in the honeycomb lattice. Apart from the DE interaction of Ni^{+}-O-Ni^{2+} configuration, Ni^{+}-O-Ni^{+} and Ni^{2+}-O-Ni^{2+} SE interactions are also possibly included in the lattice, which can thereby break the FM ordering into other magnetic phase in the low temperature range. Similar phenomenon has been also reported in previous studies, such as doped FM phase [42–44]. Specific heat measurements provide a deep perspective for understanding the magnetic phase transition. Fig. S6 (Supporting information) shows the temperature dependence of specific heat about TR-BNVO measured at 0 T. A brief overview of the $C_p(T)$ of TR-BNVO at low temperature does not show any obvious anomaly and signature of a long-range magnetic ordering, suggesting the complex magnetic interaction in the 2D honeycomb lattice, such as short-range ordering and spin-glass-like state. As displayed in Fig. S7a (Supporting information), an obvious deviation between ZFC and FC curve could be observed in TR-BNVO, which has been reported observed in many cases, such as spin-glass state, materials with competing magnetic interaction [45]. To obtain more infor-

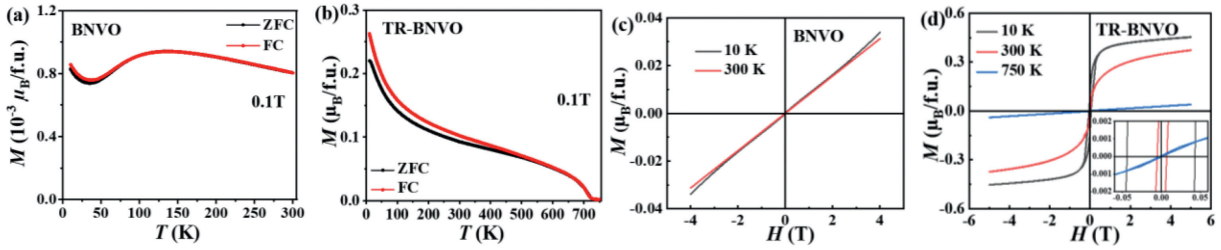

Fig. 3. (a) Temperature-dependent magnetization curves of BNVO between 10 K and 300 K measured at 0.1 T. (b) Temperature-dependent magnetization curves of TR-BNVO between 10 K and 750 K measured at 0.1 T. (c, d) Isothermal magnetization curves of BNVO and TR-BNVO at different temperature.

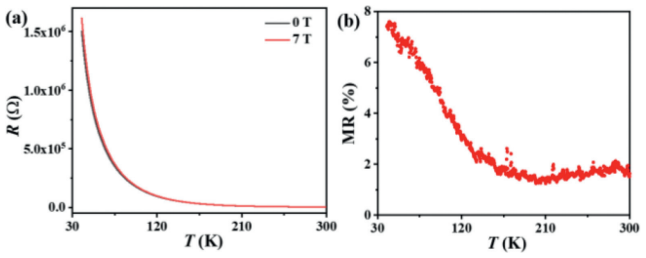

Fig. 4. (a) Temperature-dependent resistance of TR-BNVO between 40 K and 300 K at 0 and 7 T, respectively. (b) Corresponding magnetoresistance of TR-BNVO under 7 T.

mation, we further studied the magnetization curve under higher applied magnetic field (Fig. S7b in Supporting information). With increasing field, the deviation between ZFC and FC curves seems to vanish under 1 T, which is a typical characteristic of spin-glass state [46]. This indicates a possible spin-glass state of the TR-BNVO in the low temperature range. It is noteworthy that a recent theoretical breakthrough has been proposed in the prediction of quantum spin liquid (QSL) state with $S = 1/2$ system on a honeycomb lattice, where the spins are coupled to their three nearest neighbors *via* FM Ising interactions [47]. Similarly, TR-BNVO exhibits dominating FM interactions in the 2D-honeycomb lattice, making TR-BNVO a promising candidate system for the observation of QSL physics.

To intensify the understanding of the altered magnetic properties of TR-BNVO, we also measured the electronic transport properties of TR-BNVO, which is also strongly correlated to the exchange interactions. In general, transition metal oxides (TMO) display the correlations between magnetic and electronic properties: FM in TMO usually coexists with (half)-metallic conductivity, whereas insulating TMO usually exhibit AFM order [48]. Therefore, the oxygen deficient TR-BNVO in this study is expected to show a significant difference in the electronic transport properties in contrast to the as-made BNVO. As mentioned above, unreduced BNVO is a semiconductor with wide-band gap, thus it is not characterized in this case as the resistance exceeds the test limit of our equipment. As for TR-BNVO, a distinctive narrower band gap is observed, therefore we can obtain the corresponding temperature-dependent resistance (*R-T*) curve. Fig. 4a displays the *R-T* curve of TR-BNVO, in which *R* decreases uniformly with the increasing temperature, indicating a typical semiconductor behavior. In such phase, the prominently increased conductivity enables the presence of itinerant conduction electrons to take part in DE interaction, leading to the FM order of Ni spins. Given the highly insulating behavior for the unreduced BNVO mentioned above, a prevalence of AFM order is thus strongly supported. In addition, we also measured the temperature dependence of *R* for TR-BNVO under 7 T (Fig. 4a). Under high magnetic field, *R* increases over the entire temperature range, indicating a positive magnetoresistance (PMR) behavior in TR-BNVO. Fig. 4b displays the relationships of MR ($MR = (R_H - R_0)/R_0$) versus temperature at 7 T obtained from Fig. 4a, displaying the MR increases with the decreasing temperature. The PMR effect up to 7.5% at 40 K under 7 T, as observed in many compounds [49], is believed to stem from its exotic FM ground state in the 2D honeycomb lattice. In general, TMO display the correlations between magnetic and electronic properties, and TMO with MR are usually derived from chemical doping of insulators that are also magnetically ordered [50]. In this work, the original BNVO is an insulator, while TR-BNVO exhibits a semiconductor behavior with PMR, which could be ascribed to the introduction of locally abnormal Ni^+ in the honeycomb lattice like chemical doping. The MR gradually decreases with increasing temperature at first but almost remains unchanged above 150 K. According to Fig. 3b, a slight decrease of magnetic moment with increasing temperature is observed, which is ascribed to the disordered magnetic moment arrangements under impact of the thermal activation energy, leading to decreasing MR above 150 K. Thus, the PMR increases gradually with the decreasing temperature, induced by the increasing scattering of the electrons under an external field. Similar behaviors have also been discovered in other oxides with MR [51,52]. Above 150 K, it could be ascribed to the slightly change of resistance after 150 K and decreasing effect of magnetic field on the scattering of the electrons, result in a weakly temperature-dependent MR.

In conclusion, we studied the well-known Ni-based honeycomb oxides, $BaNi_2V_2O_8$ (BNVO), in which the magnetic behavior can be altered by the unusual oxidation state. The introduction of locally abnormal Ni^+ in the honeycomb lattice was also performed in BNVO by topochemical reduction (TR), yielding the TR-BNVO with mixed Ni^+-Ni^{2+} spin states in the defect-manipulated two-dimensional honeycomb lattice. The initial antiferromagnetic order was suppressed by the modulation of spin states, igniting an exotic ferromagnetic order with the transition temperature around 710 K. This magnetic phase transition is likely due to altered exchange interactions determined by the spin states, accompanied by positive magnetoresistance effect up to 7.5% at 40 K and 7 T. These features observed in TR-BNVO emphasize the key role of spin states in geometrically frustrated magnetic lattices with defect-modulated unusual ground states and exotic properties.

Declaration of competing interest

The authors declare that they have no known competing financial interests or personal relationships that could have appeared to influence the work reported in this paper.

Acknowledgments

This work was financially supported by the National Natural Science Foundation of China (NSFC, Nos. 21875287, 22090041), the Guangdong Basic and Applied Basic Research Foundation (No. 2022B1515120014).

Supplementary materials

Supplementary material associated with this article can be found, in the online version, at doi:10.1016/j.cclet.2023.108485.

References

[1] L.T. Nguyen, R.J. Cava, Chem. Rev. 121 (2021) 2935–2965.
[2] J.X. Yin, B. Lian, M.Z. Hasan, Nature 612 (2022) 647–657.
[3] C. Ahn, A. Cavalleri, A. Georges, et al., Nat. Mater. 20 (2021) 1462–1468.
[4] S. Zhao, J. Yang, Y. Han, M. Wu, M.R. Li, Chin. Chem. Lett. 34 (2023) 107355.
[5] H. Li, L. Wang, Y. Zhu, P. Jiang, X. Huang, Chin. Chem. Lett. 32 (2021) 2229–2232.
[6] A.S. Botana, V. Pardo, W.E. Pickett, M.R. Norman, Phys. Rev. B 94 (2016) 081105 (R).
[7] J. Zhang, Y.S. Chen, D. Phelan, et al., Proc. Natl. Acad. Sci. U. S. A. 113 (2016) 8945–8950.
[8] J.E. Page, M.A. Hayward, Inorg. Chem. 58 (2019) 8835–8840.
[9] C. Zhu, J. Yang, P. Shan, et al., CCS Chem. 5 (2023) 934–946.
[10] M.A. Hayward, Inorg. Chem. 58 (2019) 11961–11970.
[11] J.E. Page, H.W.T. Morgan, D. Zeng, et al., Inorg. Chem. 57 (2018) 13577–13585.
[12] Z. Xu, L. Jin, J.K. Backhaus, F. Green, M.A. Hayward, Inorg. Chem. 60 (2021) 14904–14912.
[13] Z. Xu, P.K. Thakur, T.L. Lee, et al., Inorg. Chem. 61 (2022) 15686–15692.
[14] V.V. Poltavets, K.A. Lokshin, A.H. Nevidomskyy, et al., Phys. Rev. Lett. 104 (2010) 206403.
[15] Y. Tsujimoto, C. Tassel, N. Hayashi, et al., Nature 450 (2007) 1062–1065.
[16] M. Hepting, D. Li, C.J. Jia, et al., Nat. Mater. 19 (2020) 381–385.
[17] J. Fowlie, M. Hadjimichael, M.M. Martins, et al., Nat. Phys. 18 (2022) 1043–1047.
[18] B.Y. Wang, D. Li, B.H. Goodge, et al., Nat. Phys. 17 (2021) 473–477.
[19] D. Li, K. Lee, B.Y. Wang, et al., Nature 572 (2019) 624–627.
[20] G.A. Pan, D. Ferenc Segedin, H. LaBollita, et al., Nat. Mater. 21 (2022) 160–164.
[21] C. Broholm, R.J. Cava, S.A. Kivelson, et al., Science 367 (2020) 263.
[22] J.R. Chamorro, T.M. McQueen, T.T. Tran, Chem. Rev. 121 (2021) 2898–2934.
[23] F.D.M. Haldane, Phys. Rev. Lett. 50 (1983) 1153–1156.
[24] Z. He, Y. Ueda, M. Itoh, Solid State Commun. 141 (2007) 22–24.
[25] Z. He, T. Taniyama, T. Kyômen, M. Itoh, Phys. Rev. B 72 (2005) 172403.
[26] H. Kabbour, R. David, A. Pautrat, et al., Angew. Chem. Int. Ed. 51 (2012) 11745–11749.
[27] R. David, A. Pautrat, D. Filimonov, et al., J. Am. Chem. Soc. 135 (2013) 13023–13029.
[28] R. Zhong, T. Gao, N.P. Ong, R.J. Cava, Sci. Adv. 6 (2020) eaay6953.
[29] Q. Faure, S. Takayoshi, S. Petit, et al., Nat. Phys. 14 (2018) 716–722.
[30] R. Zhong, M. Chung, T. Kong, et al., Phys. Rev. B 98 (2018) 220407 (R).
[31] N. Rogado, Q. Huang, J.W. Lynn, et al., Phys. Rev. B 65 (2002) 144443.
[32] M. Heinrich, H.A. Krug von Nidda, A. Loidl, N. Rogado, R.J. Cava, Phys. Rev. Lett. 91 (2003) 137601.
[33] W. Knafo, C. Meingast, K. Grube, et al., Phys. Rev. Lett. 99 (2007) 137206.
[34] A.A. Coelho, J. Appl. Crystallogr. 51 (2018) 210–218.
[35] L. Patra, M.R. Kishore, R. Vidya, et al., Inorg. Chem. 55 (2016) 11898–11907.
[36] R.D. Shannon, Acta. Crystallogr. A 32 (1976) 751–767.
[37] L. Cao, O. Petracic, P. Zakalek, et al., Adv. Mater. 31 (2018) e1806183.
[38] C. Zhu, G.H. Cai, C. Yuan, et al., J. Electrochem. Soc. 169 (2022) 056523.
[39] H.L. Feng, Z. Deng, C.U. Segre, et al., Inorg. Chem. 60 (2021) 1241–1247.
[40] A. Sahiner, M. Croft, S. Guha, et al., Phys. Rev. B 51 (1995) 5879–5886.
[41] J. Zhang, A.S. Botana, J.W. Freeland, et al., Nat. Phys. 13 (2017) 864–869.
[42] N. Ouled Nasser1, A. Ezaami1, M. Koubaa, et al., J. Mater. Sci. Mater. El. 29 (2018) 20658–20667.
[43] C. Nayek, S. Samanta, K. Manna, et al., Phys. Rev. B 93 (2016) 094401.
[44] D.K. Pandey, A. Modi, N.K. Gaur, J. Supercond, Nov. Magn. 33 (2020) 1433–1438.
[45] H. Zhang, B.G. Shen, Z.Y. Xu a, et al., Appl. Phys. Lett. 102 (2013) 092401.
[46] B. Pallab, P.R. Baral, R. Nath, Phys. Rev. B 98 (2018) 144436.
[47] A. Kitaev, Ann. Phys. 321 (2006) 2–111.
[48] H.L. Feng, C.J. Kang, P. Manuel, et al., Chem. Mater. 33 (2021) 4188–4195.
[49] J.G. Zhao, L.X. Yang, Y. Yu, et al., J. Appl. Phys. 103 (2008) 103706.
[50] N. Manyala, Y. Sidis, J.F. DiTusa, et al., Nature 404 (2000) 581–584.
[51] K. Huang, T. Wang, M. Jin, et al., Adv. Mater. Interfaces 8 (2021) 2002147.
[52] M.K. Chattopadhyay, S.B. Roy, S. Chaudhary, et al., Phys. Rev. B 66 (2002) 174421.